EFFECTS OF DICKE SUPERRADIANCE IN THE CONTEXT OF THE ONE-ATOM MASER

N. Nayak[a], A. S. Majumdar[b], and V. Bartzis[c]

[a&b]S. N. Bose National Centre for Basic Sciences,
Block-JD, Sector-3, Salt Lake City, Calcutta-700091, India

[c]General Department of Physics, Chemistry and Material Technology,
Technological Educational Institutions of Athens, Egaleo 12210, Greece

Abstract

We consider a micromaser model to study the influence of Dicke superradiance in the context of the one-atom maser. The model involves a microwave cavity into which two-level Rydberg atoms are pumped in pairs. We consider a random pump mechanism which allows the presence of at most one pair of atoms in the cavity at any time. We analyze the differences between the present system, called the Dicke micromaser, and an equivalently pumped conventional one-atom micromaser. These differences are attributed to the Dicke cooperativity in the two-atom system. We also show that the two-atom Dicke micromaser is equivalent to a one-atom cascade two-photon micromaser. With the introduction of a one-photon detuning, the present theory further describes a true two-photon micromaser. We discuss in detail the role of one-photon detuning in the mechanism of a one-atom two-photon micromaser. This leads us to point out that the two-atom cavity dynamics can be verified by a proper scaling of the results from an equivalent one-atom two-photon micromaser.

PACS Nos : 42.50.Dv, 42.52.+x, 32.80.-t

1. Introduction

The first experimental observation of maser action with just one atom in the so-called micromaser [1] renewed interest in the subject extensively as it opened possibilities of observing cavity-QED effects which are purely of quantum mechanical origin. Indeed, one of the results of the much discussed Jaynes-Cummings interactions [2], the quantum revival of the oscillations in the atomic population, has been observed in the micromaser device [3]. The micromaser device [1] consists of a high-Q superconducting cavity cooled down to sub-Kelvin temperatures into which Rydberg atoms in the upper of the two masing levels are pumped randomly but one at a time. A clever velocity selector decides a fixed flight time τ through the cavity for every atom. The repetition time $\bar{t}_R$, τ and t_{cav}, the duration in which the cavity is empty of atom, satisfy $\bar{t}_R = \tau + t_{cav}$ with $\tau \ll t_{cav}$. This is the basis of the one-atom maser theories [4-6] with the further assumption of strictly single-atom events.

However, the above arrangements in the experiments [1,3] cannot eliminate overlap of flight times through the cavity of successive atoms completely, which of course, is less than 1%. This has been one of the obstacles in realizing certain predictions of one-atom maser theories [4,5] such as number states of the cavity radiation field. Another limiting factor is the dissipative mechanism acompanying the coherent atom-field interaction [6]. The results in [6] show that the effects of the dissipative mechanism can be minimized by increasing the Q factor of the cavity and by decreasing its temperature. But the pump mechanism has not been able to eliminate traces of two atom events in one-atom maser dynamics. Hence it has become necessary to explain the effect of such two-atom events on the photon statistics of the cavity field. Various models incorporating multiple atomic events have been proposed [7–13]. The basic difference between such models and one-atom maser theory [4-6] is the Dicke atomic cooperative effect [14,15] acompanying the

multiple atomic events. Thus, in order to understand the limitations of maser theories based on strictly single atom events [4-6], it is necessary to quantify the effect of atomic cooperation. For this purpose we propose the following model.

We consider a fixed number of atoms entering the cavity with a constant flight time through it, but with random time gaps between successive such events. The cooperative nature [12] of the interaction of the atoms with the cavity field shall be fully reflected in the photon statistics. In this paper we consider atoms being pumped in pairs into the cavity. We limit the number of atoms to two just for the sake of simplicity which can be easily generalized to a larger number. Both the atoms are taken to be in their upper states when they enter the cavity. The arrival of the pair at the cavity is assumed to be Poissonian. We thus have $\bar{t}_R = \tau + \bar{t}_{cav}$ with $t_R = 1/\bar{R}$. We assume τ to be a fixed duration for every pair of atoms, and hence, t_{cav} is random. $\bar{R}$ is now a Poisson average of R pairs of atoms pumped into the cavity in one second. Due to cooperative interaction of the pair of atoms with the cavity field, we will find its dynamics with $\bar{R}$ pairs of atoms pumped into the cavity per second in the present case being different from the one-atom maser pumped with $2\bar{R}$ atoms into the cavity per second. This is due to the superradiance effects [14,15] which will be manifested in the steady-state photon statistics. For these reasons, we call the present system a "Dicke micromaser".

It is rather a difficult task to achieve such a model experimentally. However, we will show in the following that the present model is closely related to a one-atom two-photon micromaser [16-18]. This is a key result of this paper. Two-photon micromaser action with one atom has been experimentally demonstrated [16]. Thus the model we are considering to show the atomic cooperative effects is not beyond experimental verification.

The organization of the paper is as follows. In the section 2, we present the microscopic Hamiltonian and the Dicke states involved in the micromaser action. The equations of motion are derived in section 3. We derive and discuss the photon statistics in section

4. The present system is compared with the two-photon micromasers in section 5. We conclude the paper in section 6.

2. The Model

A pair of Rydberg atoms in the upper of their two levels a and b enter the cavity at $t = 0$. We assume that the atomic transition frequency is in resonance with the cavity mode frequency ω. Both the atoms take the time τ to travel across the cavity. During this time, the evolution of the system comprising of the two atoms and the single eigen mode of the microwave cavity is governed by the Hamiltonian

$$H = H_0 + H_I \tag{1a}$$

where

$$H_0 = \omega(S_1^Z + S_2^Z + a^\dagger a) \tag{1b}$$

as we consider resonance condition between atomic transition frequencies and the cavity frequency. H_I is the Jaynes-Cummings Hamiltonian [2].

$$H_I = g\sum_{i=1}^{2}(S_i^+ a + S_i^- a^\dagger) \tag{1c}$$

We assume that the atom-field coupling constant g is the same for each atom. The atomic operators obey the relations $[S_i^+, S_j^-] = 2S_i^Z\delta_{ij}$ and $a(a^\dagger)$ is the photon annihilation (creation) operator obeying the commutation relation $[a, a^\dagger] = 1$. In the frame rotating at H_0, we have $H = H_I$.

It is convenient to represent the two-atom system by a Dicke system as both the atoms interact with the same cavity field simultaneously. In doing so, we however, neglect the dipole-dipole interaction as the microwave cavity dimensions are much large compared to

particle wavelengths. Defining the collective operators $S^{\pm} = \sum_{i=1}^{2} S_i^{\pm}$, Eq.(1c) takes the form

$$H_I = g(S^+ a + S^- a^\dagger) \tag{2}$$

which is clearly invariant by atomic permutation. Both the atoms are in their respective upper states at $t = 0$ and hence, the state representing the atomic system $|a, a\rangle$ is also invariant under atomic permutation. So it remains in a symmetrical state at all times. These are known as Dicke states with maximum cooperative number $J = 1$ (we have a two-atom system) and these states are isomorphous to angular momentum states with principal angular momentum $J = 1$. These states, represented by $|J, M\rangle$, are generated by

$$S^-|J, M\rangle = \sqrt{(J + M)(J - M + 1)}|J, M - 1\rangle$$

and

$$S^+|J, M\rangle = \sqrt{(J + M + 1)(J - M)}|J, M + 1\rangle \tag{3}$$

The level $|J, M\rangle$ is nondegenerate and has atomic energy $M\omega$. As $-J \leq M \leq J$, this has $2J + 1$ states, and in the present case, the number of states is three. Since J is a constant here, we represent $|J, M\rangle \equiv |M\rangle$.

Thus, the pair of two-level atoms can be represented by a three-level system of the Dicke states $|M = 1\rangle$, $|M = 0\rangle$, and $|M = -1\rangle$, having energy ω, 0, and $-\omega$ respectively. This allows us to write the Hamiltonian in Eq.(2) in the matrix form

$$H_I = \begin{pmatrix} 0 & g\sqrt{2(n-1)} & 0 \\ g\sqrt{2(n-1)} & 0 & g\sqrt{2n} \\ 0 & g\sqrt{2n} & 0 \end{pmatrix} \tag{4}$$

where n represents the photon number of the cavity field. Eq.(4) resembles the case for a two-photon process in a three-level system [19]. Following the method in [19], we can

obtain the eigenvalues and eigenstates of the interaction of the Dicke states with the cavity radiation field. The eigenvalues

$$\begin{aligned} \lambda_0 &= 0, \\ \lambda_+ &= g\sqrt{2(2n-1)}, \\ \lambda_- &= -g\sqrt{2(2n-1)}, \end{aligned} \tag{5}$$

and its states are, respectively,

$$\begin{aligned} |0,n\rangle &= x_1^{(n)}|1,n-2\rangle + y_1^{(n)}|0,n-1\rangle + z_1^{(n)}|-1,n\rangle, \\ |+,n\rangle &= x_2^{(n)}|1,n-2\rangle + y_2^{(n)}|0,n-1\rangle + z_2^{(n)}|-1,n\rangle, \\ |-,n\rangle &= x_3^{(n)}|1,n-2\rangle + y_3^{(n)}|0,n-1\rangle + z_3^{(n)}|-1,n\rangle, \end{aligned} \tag{6}$$

where $|1,n\rangle$, $|0,n\rangle$ and $|-1,n\rangle$ are the composite Dicke and field states, and

$$x_1^{(n)} = \sqrt{\frac{n}{2n-1}},\ \ y_1^{(n)} = 0,\ \ z_1^{(n)} = -\sqrt{\frac{n-1}{2n-1}}, \tag{7a}$$

$$x_2^{(n)} = -\sqrt{\frac{n-1}{4n-2}},\ \ y_2^{(n)} = -\frac{1}{\sqrt{2}},\ \ z_2^{(n)} = -\sqrt{\frac{n}{4n-2}}, \tag{7b}$$

$$x_3^{(n)} = -\sqrt{\frac{n-1}{4n-2}},\ \ y_3^{(n)} = \frac{l}{\sqrt{2}},\ \ z_3^{(n)} = -\sqrt{\frac{n}{4n-2}}. \tag{7c}$$

The states $|+,n\rangle$, $|-,n\rangle$ and $|0,n\rangle$ can be called as dressed states of the interaction of the Dicke states with the cavity field.

3. Derivation of the equations of motion

Using the dressed states in Eq.(6) as the basic states, the equation of motion

$$\dot{\rho} = -i[H,\rho] \tag{8}$$

can be derived easily [19]. ρ represents the composite atom-field system having the initial conditions

$$\rho_{i,j}^{(n)}(t=0) \equiv \langle i,n|\rho|j,n\rangle = x_i^{(n)} x_j^{(n)} P_{n-2} \tag{9}$$

where P_n is the photon distribution function of the cavity radiation field. In writing Eq.(6), we have neglected the influences of the atomic as well as the cavity reservoirs on the dynamics. These effects can play a crucial role in the one-atom micromaser [6]. However, these influences have been shown to be negligible [6] for a cavity having very high Q and at very low temperatures and a low atomic pump rate. Eq.(8) represents such a system.

The time-dependent solutions for the density matrix elements can be written as

$$\rho_{i,j}^{(n)}(t) = P_{n-2} x_i^{(n)} x_j^{(n)} e^{-i(\lambda_i^{(n)} - \lambda_j^{(n)})t}, \tag{10}$$

$$i,j \ \equiv 0,+,-.$$

By inverting the matrix which expresses the dressed states as a linear superposition of the Dicke states, we can obtain the Dicke states $|i,n\rangle$, $i = 1,0,-1$, in terms of the dressed states. Using these relations and Eq.(10), we obtain the density matrix elements in the Dicke state basis. We follow these steps to get the P_n at $t = \tau$, which is given by the trace

$$P_n(\tau) = \sum_{M=-1}^{+1} \langle M,n|\rho|M,n\rangle. \tag{11}$$

We thus have

$$P_n(\tau) = \Theta_1^{(n)}(\tau) P_n + \Theta_2^{(n)}(\tau) P_{n-1} + \Theta_3^{(n)}(\tau) P_{n-2} \tag{12}$$

where

$$\Theta_1^{(n)}(\tau) = \frac{(n+2)}{(4n+3)}(x_1^{(n+2)})^2 + \frac{(n+1)}{(4n+6)}\Big((x_2^{(n+2)})^2 + (x_3^{(n+2)})^2\Big)$$
$$-\frac{2\sqrt{(n+2)(n+1)}}{\sqrt{(4n+3)(4n+6)}}\Big(x_1^{(n+2)} x_2^{(n+2)} Re.(e^{i\lambda_+^{(n+2)}\tau}) + x_1^{(n+2)} x_3^{(n+2)} Re.(e^{i\lambda_-^{(n+2)}\tau})\Big)$$

$$+\frac{2(n+1)}{(4n+6)}x_2^{(n+2)}x_3^{(n+2)}Re.(e^{-i(\lambda_+^{(n+2)}-\lambda_-^{(n+2)})\tau}), \tag{13a}$$

$$\Theta_2^{(n)}(\tau)=\frac{1}{2}\Big((x_2^{(n+1)})^2+(x_3^{(n+1)})^2\Big)-x_2^{(n+1)}x_3^{(n+1)}Re.(e^{-i(\lambda_+^{(n+1)}-\lambda_-^{(n+1)})\tau}), \tag{13b}$$

$$\begin{aligned}\Theta_3^{(n)}(\tau)&=\frac{n-1}{2n-1}(x_1^{(n)})^2+\frac{n}{4n-2}\Big((x_2^{(n)})^2+(x_3^{(n)})^2\Big)\\&+\frac{\sqrt{2n(n-1)}}{(2n-1)}\Big(x_1^{(n)}x_2^{(n)}Re.(e^{i\lambda_+^{(n)}\tau})+x_1^{(n)}x_3^{(n)}Re.(e^{i\lambda_-^{(n)}\tau})\Big)\\&+\frac{2n}{4n-2}x_2^{(n)}x_3^{(n)}Re.(e^{-i(\lambda_+^{(n)}-\lambda_-^{(n)})\tau}).\end{aligned} \tag{13c}$$

The change in P_n at $t=\tau$ is then $\delta P_n=P_n(\tau)-P_n$ where P_n is the photon distribution function at the time of a pair of atoms entering the cavity. For a time $\triangle t$ such that $\tau\ll\triangle t\ll t_p$, where t_p is the cavity photon lifetime, we have

$$\triangle P_n=\delta P_n R\triangle t \tag{14}$$

where R is the number of pairs of atoms passing through the cavity in one second

The coarse-grained time derivative due to gain from the atomic interaction is given by

$$\frac{dP_n}{dt}|_{gain}=R\Big((\Theta_1^{(n)}-1)P_n+\Theta_2^{(n)}P_{n-1}+\Theta_3^{(n)}P_{n-2}\Big). \tag{15}$$

Eq.(15) represents the dynamics during time τ. During the time lapse t_{cav}, between the flights of two successive pairs of atoms, the cavity field interacts with its reservoir, and its equation of motion is given by [6]

$$\dot{P}_n|_{loss}=2(n+1)(\bar{n}_{th}+1)\kappa P_{n+1}-2\kappa(n+\bar{n}_{th}+2n\bar{n}_{th})P_n+2n\kappa\bar{n}_{th}P_{n-1} \tag{16}$$

where $\kappa=(2t_p)^{-1}$ is the cavity bandwidth, and $\bar{n}_{th}$ is the thermal photon present in the cavity. Under the coarse-graining assumptions, the complete equation of motion combines Eqs.(15) and (16) additively. This assumption has been seen to be valid [20] for a random

input of atoms into the cavity, which is the case we are studying in this paper. We thus have,

$$\dot{P}_n = \dot{P}_n|_{gain} + \dot{P}_n|_{loss} \tag{17}$$

4. Steady-state photon statistics

The equation of motion for P_n, given by Eq.(17), involves P_{n-2}, and this makes it difficult to get a steady-state solution by the method followed in case of the one-atom micromaser [6]. However, following Risken [21], Eq.(17) can be recast in a tri-diagonal matrix equation involving the two-component vector $T_n = \begin{pmatrix} P_{2n} \\ P_{2n+1} \end{pmatrix}$, which provides an expression for T_n in the form of matrix continued fractions. Eq.(17) directly gives an expression for P_1 in terms of P_0, and P_0 can be determined from the normalization condition. This completes the determination of P_n. But numerical evaluations of P_n go out of control due to extremely slow convergence of the matrix continued fractions.

Hence, we follow the method given below, which we find computationally efficient. First, we set n at a value $n = n_{max}$, say, and write all the P_n in a vector

$$\vec{X} = \{P_0, P_1, P_2, ..., P_{n_{max}}\}^T \tag{18}$$

This vector obviously has $n_{max} + 1$ elements. We get n_{max} equations involving $P_0, P_1, P_2, ..., P_{n_{max}}$ from Eq.(17). With the normalization condition

$$\sum_{n=0}^{n_{max}} P_n = 1 \tag{19}$$

we get the equation

$$M\vec{X} = \vec{I} \tag{20}$$

where M is a $(n_{max}+1) \times (n_{max}+1)$ matrix and $\vec{I}$ is another vector having again $n_{max}+1$ elements

$$\vec{I} = \{0, 0, 0, ..., 1\}^T \tag{21}$$

The solution

$$\vec{X} = M^{-1}\vec{I} \tag{22}$$

gives all P_n for $0 \leq n \leq n_{max}$.

We analyze the photon statistics of the cavity field by numerically evaluating its first and second moments, that is,

$$< n >= \sum_{n=0}^{n_{max}} nP_n \tag{23}$$

proportional to the intensity of the cavity field and its normalized variance

$$v = \sqrt{\frac{< n^2 > - < n >^2}{< n >}} \tag{24}$$

$v = 1$ for a coherent state field, and thus, $v < 1$ indicates the nonclassical nature of the cavity field. The process is repeated for a higher value of n_{max} and the corresponding $< n >$ and v are compared with those obtained from the earlier value of n_{max}. If they agree to a desired accuracy, the process is stopped, and we have the numerical values of the photon distribution function P_n, as well as the average $< n >$ and variance v.

The results are displayed in Figs.1-3. For the convenience of describing the micromaser action, we define the pump parameter

$$D = \sqrt{N} g\tau \tag{25}$$

where $N = \bar{R}/2\kappa$ is the number of pairs of atoms that pass through the cavity in a photon lifetime $(2\kappa)^{-1}$. The patterns in the variation of $< n >$ and v as $D(\propto \tau)$ changes, can be understood from the dynamics [22] of a collection of two-level atoms interacting with the radiation field of a single mode cavity with each atom being coupled to the cavity field by the Jaynes-Cummings interaction [2]. For a two-atom case with initial condition $J = 1$, it has been shown in [22] that the dynamics is controlled by a d.c. term with a prefactor of the order of P_n/n and terms oscillating at the first and second harmonic of the Rabi frequancy $2g\sqrt{n + 3/2}$ of the interaction Hamiltonian in Eq.(1c) and having

prefactors proportional to P_n and P_n/n respectively. In the single-atom case [23] (Jaynes-Cummings model), the well known dynamics is controlled by only one term having the prefactor P_n and oscillating at the Rabi frequency $2g\sqrt{n+1}$ of the Jaynes-Cummings interaction [2]. These differences make the present results different, in general, from the one-atom micromaser action. Figs.1-3 show the differences clearly where we compare the results for the present Dicke micromaser for $\bar{N} = 100$ with the one-atom micromaser action [4-6] with a pump rate $\bar{N} = 200$. The numerical values of the two pump rates make the total number of atoms that pass through the two cavities having the same Q equal, and thus, justifies the comparison between the two systems. Fig.2a shows that the superradiance nature of the interaction in Eq.2 makes the threshold values of D lower compared to the one-atom micromaser. The differences between the two systems become predominant for higher values of D, that is, for longer interaction times. This is evidently due to the cooperative interaction becoming more important for longer interaction times. Thus, we notice in Fig.1 that $< n >$ is in general higher compared to the one-atom micromaser for longer τ.

The variance in the cavity field is in general different in the two systems. It is generally very high near threshold, and hence, the sharp peaks in v at threshold appear at different values of D in the two systems as depicted in Fig.2b. We also notice in Fig.2b that the cavity field gets nonclassical properties ($v < 1$) for different ranges of D in the two systems. The photon distribution function also has different shapes as shown in Figs.3, which clearly shows that the nature of the field depends clearly on the nature of the pump. For example, in Fig.3a, the field in the one-atom case is sub-Poissonian, while the field in the two-atom case is super-Poissonian. The field characteristics are vice-versa in Fig.3c. However, the P_n in the present case do not indicate any existence of the so-called trapped states [4-6]. The Rabi frequencies in the two-atom Dicke system, represented by the eigen values λ_0, λ_+ and λ_- do not provide clear conditions for the trapped states as

one gets in the case of the one-atom micromaser [6]. There the conditions are essentially zeros of the function $Sin\sqrt{n+1}x$, x being the dimensionless atom-field interaction time. The trapped states, are however, washed out by occasional presence of two atoms in the cavity of the one-atom maser [7,8]. Thus the present analysis gives an easy and transparent understanding of the disappearance of trapped states in multi-atom events.

5. Comparison with one-atom two-photon micromaser

The Dicke micromaser studied in the present paper has similarities with the dynamics of a one-atom two-photon micromaser [16] involving pumping of atoms, individually into a microwave cavity where the atoms make a two-photon transition [19] from the upper to lower level via an intermediate level. This is because the Dicke atomic system with $J = 1$ is equivalent to a one-atom three-level system with the middle level having equal frequency of separation ω from the upper and the lower levels. It may be noted here that ω is the transition frequency of the individual two-level atoms in the Dicke system. If the cavity eigenmode is in resonance with the two degenerate atomic transitions, and in addition, if they have dipole moments of equal strength, then the present theory can be employed to explain the dynamics of the two-photon cascade micromaser. In other words, the results in Figs.1-3 can represent a one-atom two-photon cascade micromaser if we set the coupling constants of the two degenerate transitions $g_1 = g\sqrt{2}$. The factor $\sqrt{2}$ in the Dicke system represents its cooperative nature [14].

We need not stop at this comparison. A Dicke micromaser with pumping of three atoms at a time (all in their upper masing levels) will be equivalent to a degenerate five-photon cascade micromaser, and so on.

However, a true two-photon process involves non-resonant one-photon transitions. If ω_1 and ω_2 are two atomic transitions, and ν is the cavity mode frequency, then a true two-photon process should have large detunings $\triangle_1 = \omega_1 - \nu$ and $\triangle_2 = \nu - \omega_2$, that is,

$\triangle_1$, $\triangle_2 \gg g_1$. A two-photon resonance means $\triangle_1 + \triangle_2 = 0$, or $\omega_1 + \omega_2 = 2\nu$. In the cascade two-photon micromaser discussed above, we have $\triangle_1 = \triangle_2 = 0$. An extensive comparison of cavity-QED of cascade two-photon with true two-photon processes can be found in [19] where it has been shown that the two dynamics are, in general, different.

The present approach can also be applied to such a two-photon micromaser if we can accomodate the one-photon detuning in the derivation of the photon distribution function. This amounts to just setting the matrix elements $[H_I]_{1,1} = [H_I]_{3,3} = -\triangle$ in Eq.4. For simplicity, we set $g_1 = g\sqrt{2}$ here also. We present the photon statistics for the two photon micromaser for various values of $\triangle$ in Figs.4. We find that the operational characteristics are strongly dependent on $\triangle$. We also notice that as $\triangle$ increases, the theory recovers the results for a two-photon micromaser derived by using an effective two-level Hamiltonian, a derivation and discussion of which can be found in [19].

For smaller values of $\triangle$, we notice wriggles in the variation of $< n >$ versus D in Fig.4a. These wriggles begin at a value of $D(\propto \tau)$ and persist as it is further increased. The value of D at which the wriggles begin to appear increases with $\triangle$. In other words, the smooth variations in $< n >$ as in the case of an *effective two-level system* [17,18], occur for values of D having an upper bound which increases with $\triangle$. Such characteristics have been discussed in detail in the context of the two-photon Jaynes-Cummings model in [19]. In addition to the above results, we also notice that the thresholds shift to higher values of D as $\triangle$ increases, and also, the range of D between two successive thresholds also increases with the one-photon detuning. The cavity field usually has sub-Poissonian photon statistics ($v < 1$) between successive thresholds, and thus with a larger detuning, this model provides sub-Poissonian fields for wider range of D as shown in Fig.4b.

6. Conclusion

We have presented a theory for a two-atom Dicke micromaser and have brought out

the role played by the Dicke cooperativity on the micromaser action. Though at first glance it may look that the Dicke micromaser results mimic that for an equivalently pumped one-atom maser, the two systems are in general different. At places, however, the two systems have similar trends, an example of which can be seen in Fig.3b. We further show that the micromaser dynamics involving the three-level Dicke atomic system is formally equivalent to a one-atom cascade two-photon micromaser. Interestingly, we note that the two one-photon coupling constants in the two-photon cascade transition has to scale $\sqrt{2}$ times of the one-atom coupling constants in the Dicke system for the two micromaser actions to have identical results. As mentioned above, this factor of $\sqrt{2}$ originates from the cooperative nature of the Dicke system. With the introduction of a one-photon detuning in the two-photon process, the present approach also describes a one-atom two-photon micromaser. We have discussed in detail the role of the one-photon detuning in a two-photon micromaser action. Thus the Dicke superradiance effects can be quantitatively evaluated by scaling, as mentioned above, the results from the one-atom two-photon micromaser [16].

Thus the Dicke micromaser model discussed in this paper is not beyond the scope of experiments for verifying its results. The present paper gives the clue to verify results from micromaser actions involving pump mechanisms like the one studied here, which are rather difficult to achieve experimentally. This suggests a way to experimentally demonstrate the two-atom cavity-QED results [22] in a one-atom two-photon micromaser [16]. It may be recalled that the one-atom micromaser [1] demonstrated the phenomenon of quantum revival [23]. The same techniques may be employed in the case of the one-atom two-photon micromaser [16] and a proper scaling of its results should demonstrate the two-atom cavity-QED results [22].

REFERENCES

1. D. Meschede, H. Walther and G. Muller, Phys. Rev. Lett. **54**, 551 (1985).
2. E. T. Jaynes and F. W. Cummings, Proc. IEEE **51**, 89 (1963).
3. G. Rempe, H. Walther and N. Klein, Phys. Rev. Lett. **58**, 353 (1987).
4. P. Filipowicz, J. Javanainen and P. Meystre, Phys. Rev. A **34**, 3077 (1986).
5. L. A. Lugiato, M. O. Scully and H. Walther, Phys. Rev. A **36**, 740 (1987).
6. N. Nayak, Opt. Commun. **118**, 114 (1995).
7. M. Orszag, R. Ramirez, J. C. Retamal and C. Saavedra, Phys. Rev. A **49**, 2933 (1994).
8. E. Wehner, R. Seno, N. Sterpi, B. -G. Englert and H. Walther, Opt. Commun. **110**, 655 (1994).
9. G. M. D'Ariano, N. Sterpi and A. Zucchetti, Phys. Rev. Lett. **74**, 900 (1995).
10. M. Elk, Phys. Rev. A **54**, 4351 (1996).
11. M. I. Kolobov and F. Haake, Phys. Rev. A **55**, 3033 (1997).
12. K. An, J. J. Childs, R. R. Dasari and M. S. Feld, Phys. Rev. Lett. **73**, 3375 (1994).
13. H. J. Carmichael and B. C. Sanders, Phys. Rev. A **60**, 2497 (1999).
14. R. H. Dicke, Phys. Rev. **93**, 99 (1954).
15. J. M. Raimond, P. Goy, M. Gross, C. Fabre and S. Haroche, Phys. Rev. Lett. **49**, 1924 (1982).

16. M. Brune, J. M. Raimond, P. Goy, L. Davidovich and S. Haroche, Phys. Rev. Lett. **59**, 1899 (1987).

17. L. Davidovich, J. M. Raimond, M. Brune and S. Haroche, Phys. Rev. A **36**, 3771 (1987).

18. I. Ashraf, J. Gea-Banacloche and M. S. Zubairy, Phys. Rev. A **42**, 6704 (1990).

19. V. Bartzis and N. Nayak, J. Opt. Soc. Am. B **8**, 1779 (1991).

20. J. Bergou, L. Davidovich, M. Orszag, C. Benkert, M. Hillary and M. O. Scully, Phys. Rev. A **40**, 5073 (1989); L. Davidovich, S. -Y. Zhu, A. Z. Khoury and C. Su, Phys. Rev. A **46** 1630 (1992).

21. H. Risken, *Fokker - Planck Equations* (Springer - Verlag, Berlin, 1984), p. 200.

22. G. Ramon, C. Brif and A. Mann, Phys. Rev. A **58**, 2506 (1998).

23. N. Nayak, R. K. Bullough, B. V. Thompson and G. S. Agarwal, IEEE J. Quant. Electron QE **24**, 1331 (1988) and references therein.

FIGURE-CAPTIONS

Fig.1

The cavity field intensity, proportional to $< n >$, versus the pump parameter D. $\bar{n}_{th} = 0.1$. $\bar{N} = 100$ and 200 for the Dicke micromaser (a) and one-atom micromaser (b) respectively. This makes the total number of atoms that pass through the cavity in the two systems equal. The curve (b) is shifted upwards by 150 for clarity.

Fig.2a

Variation in $< n >$ with respect to D for shorter interaction time. The parameters are same as in Fig.1. The full and broken curves are for the Dicke micromaser and one-atom micromaser respectively.

Fig.2b

Variation of v with D. The other parameters are same as in Fig.2a.

Fig.3a

Photon distribution function for $D = 25$. The other parameters are same as in Figs.2. $P(n)$ is sub-Poissonion ($v = 0.60761$) in the case of one-atom micromaser (broken curve), and is super-Poissonian ($v = 1.27596$) in the case of Dicke micromaser.

Fig.3b

$P(n)$ for $D = 50$. The other parameters are same as in Fig.3a. For both the cases, $P(n)$ is super-Poissonian at this value of D. $v = 1.09944$ (broken curve) and $v = 1.15871$ (full curve).

Fig.3c

$D = 400$. $P(n)$ is sub-Poissonian ($v = 0.22911$) in the Dicke micromaser system (full curve). One-atom micromaser (broken curve) provides a super-Poissonian ($v = 1.05726$)

in this case.

Fig.4a

$< n >$ versus D for a two-photon micromaser for three different values of the one-photon detuning $\triangle$. $\bar{n}_{th} = 0.1$ and $\bar{N} = 100$. $\triangle = 100$ (curve (a)), $\triangle = 150$ (curve (b)), and $\triangle = 300$ (curve (c)). For clarity, the curves (b) and (c) are shifted upwards by 40 and 80 respectively.

Fig.4b

Variation of v with D for a two-photon micromaser. The other parameters are same as in Fig.4a. Here, the curves (b) and (c) are shifted by 4 and 8 respectively, for clarity.

Figure 1

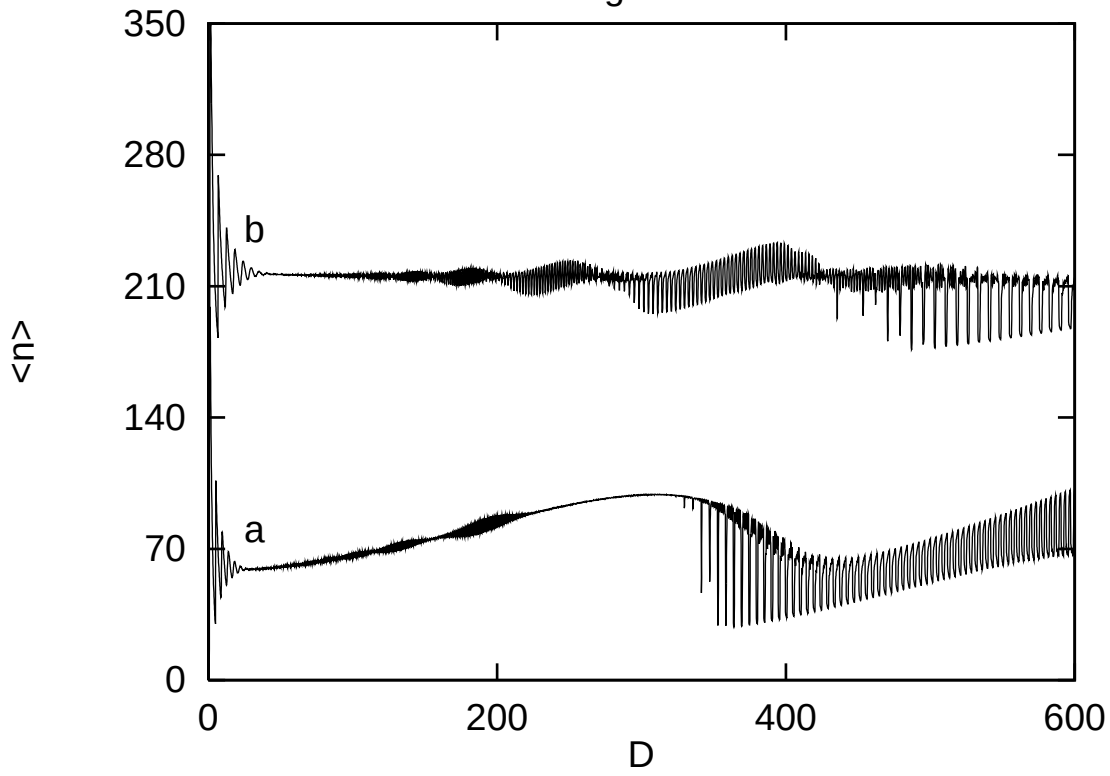

Figure 2a

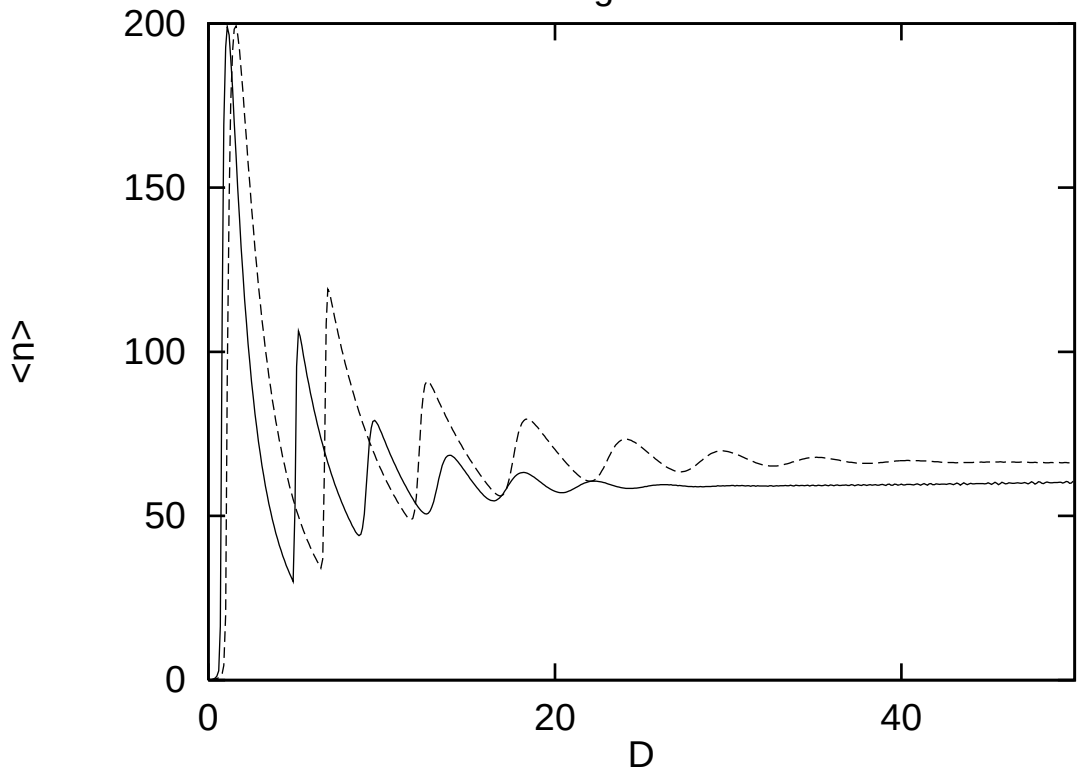

Figure 2b

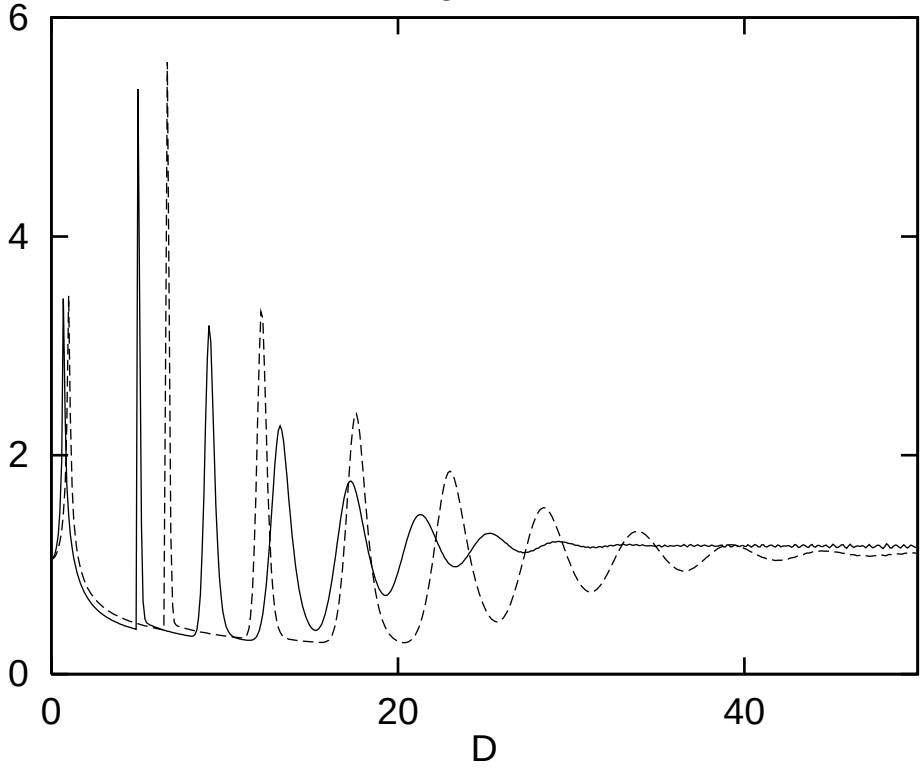

Figure 3a

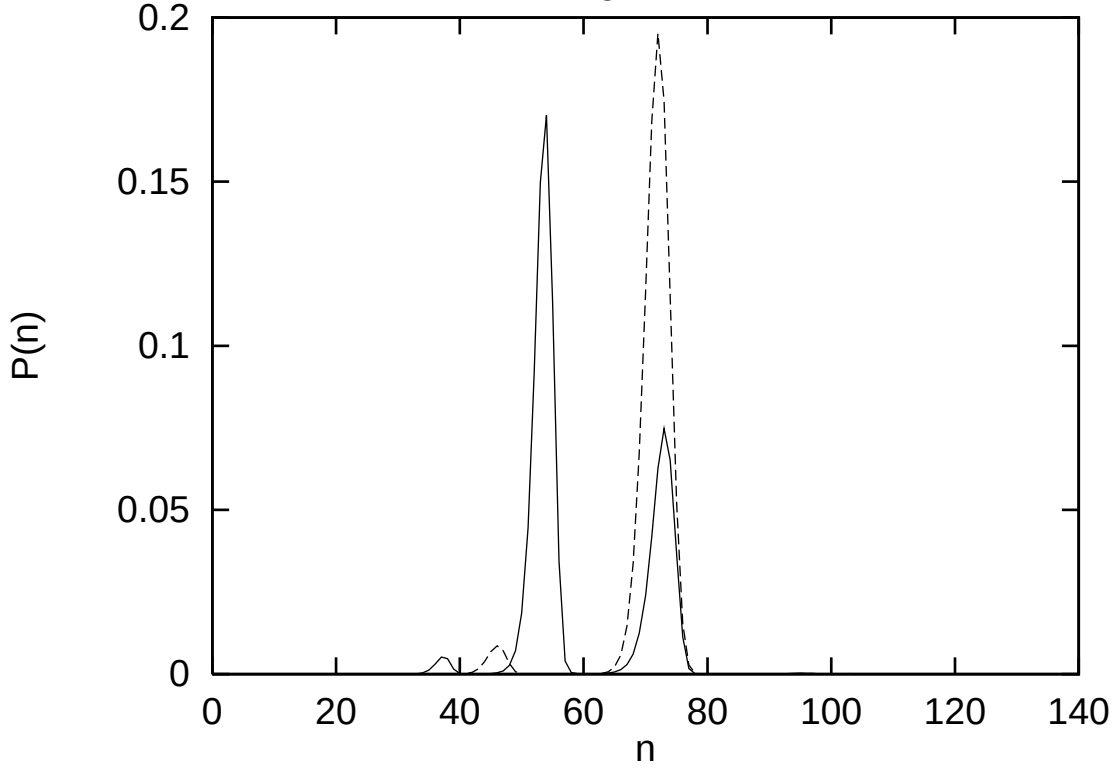

Figure 3b

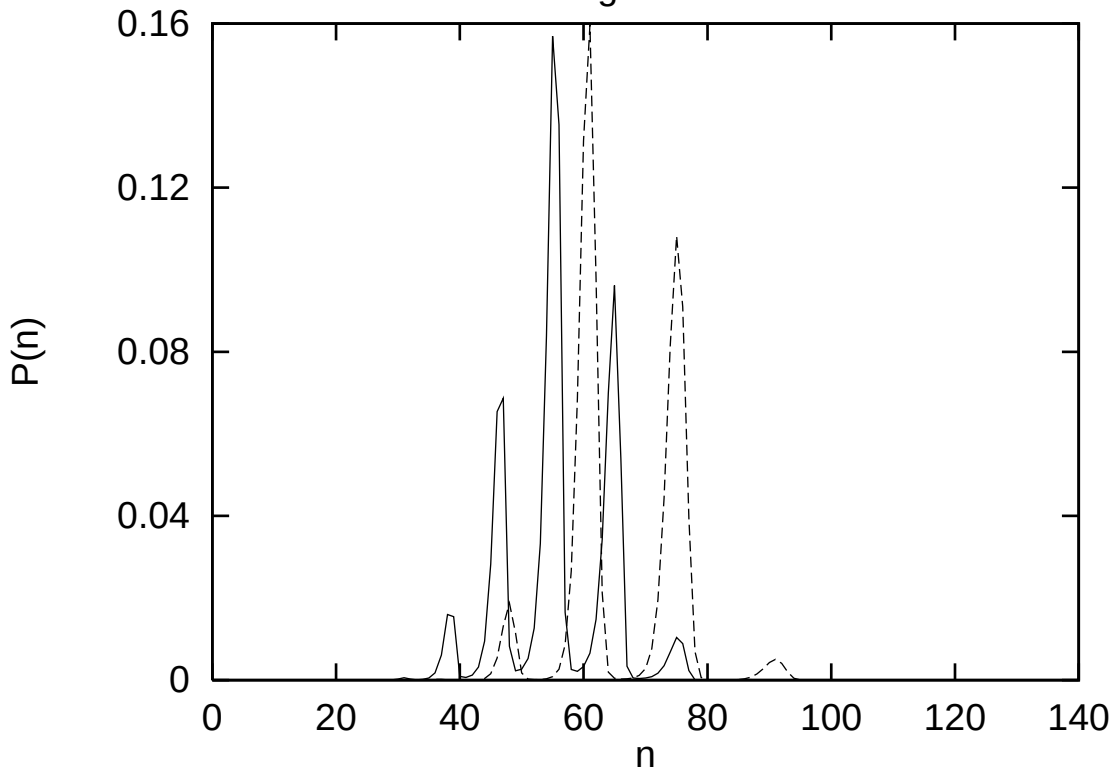

Figure 3c

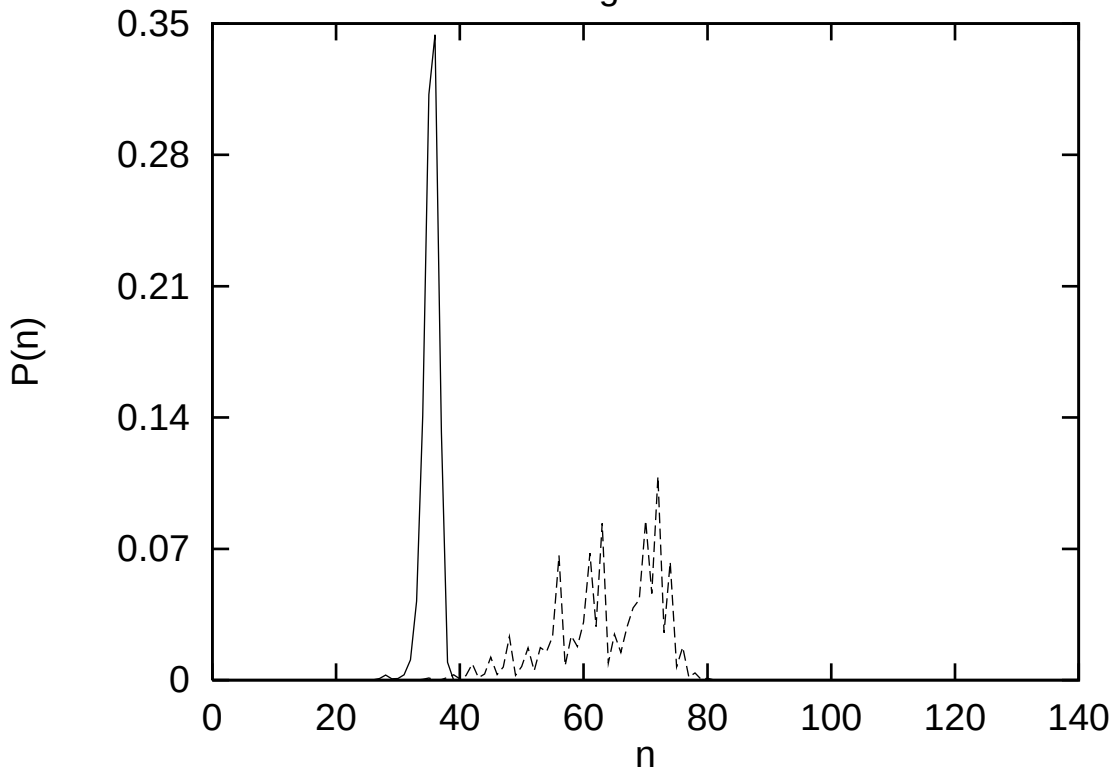

Figure 4a

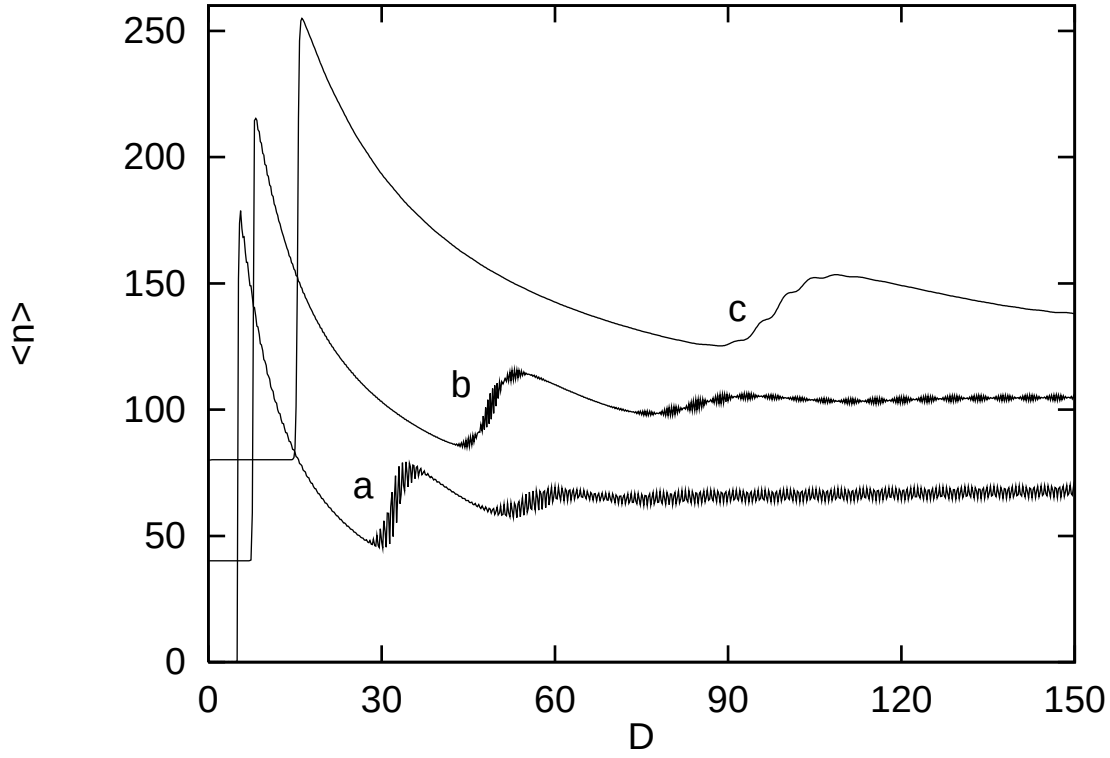

Figure 4b